ADVANCED ENERGY MATERIALS
www.advenergymat.de

Impact of Local Microenvironments on the Selectivity of Electrocatalytic Nitrate Reduction in a BPM-MEA System

*Po-Wei Huang, Hakhyeon Song, Jaeyoung Yoo, Danae A. Chipoco Haro, Hyuck Mo Lee, Andrew J. Medford, and Marta C. Hatzell**

Electrochemical nitrate reduction reaction (NO_3RR) has garnered increasing attention as a pathway for converting a harmful pollutant (nitrate) into a value-added product (ammonia). However, high selectivity toward ammonia (NH_3) is imperative for process viability. Optimizing proton availability near the catalyst is important for achieving selective NH_3 production. Here, the aim is to systematically examine the impacts of proton availability on NO_3RR selectivity in a bipolar membrane (BPM)-based membrane electrode assembly (MEA) system. The BPM generates a proton flux from the membrane toward the catalyst during electrolysis. Thus, the BPM-MEA system can modulate the proton flux during operation. The impact of interposer layers, proton scavenging electrolytes (CO_3^{2-}), and catalyst configurations are also examined to identify which local microenvironments favor ammonia formation. It is found that a moderate proton supply allows for an increase in ammonia yield by 576% when compared to the standard MEA setup. This also results in a high selectivity of 26 (NH_3 over NO_2^-) at an applied current density of 200 mA cm^{-2}.

1. Introduction

Nitrogen-based fertilizer is essential for agriculture, however, nitrate runoff into groundwater results in serious health issues such as infant methemoglobinemia and cancer.[1] Due to the rising demand for fertilizer use, the treatment of nitrate-contaminated waters is a growing concern. Nitrate removal occurs using physicochemical methods like ion exchange resins, which are effective in extracting nitrate from the feed stream. These physiochemical methods however generate a significant amount of waste brines that contain high concentrations of nitrate (ranging from 1000 to 9000 ppm NO_3^--N).[2] Disposal of this concentrated waste stream is a significant challenge. In this context, catalytic or electrocatalytic conversion of nitrate to harmless (N_2) or value-added (NH_3), has garnered great attention.[1d,3] The appeal of electrocatalysis is in the seamless integration with renewable energy sources, providing a means to remediate nitrogen waste with non-fossil-based energy sources.

Electrocatalytic conversion depends on fully understanding the nitrate reduction reaction (NO_3RR). There has been significant progress in understanding the NO_3RR reaction mechanisms, and in tuning selectivity. Reports have also suggested that ammonia can be produced at Faradaic efficiencies (FE) exceeding 90%.[4] However, most investigations are conducted under restrictive conditions, including low current density (H-type cell), strong alkaline conditions (pH >14), and with elevated nitrate concentration.[5] There have been limited investigations to assess the feasibility of NO_3RR under high currents, in flow cells, and with wastewater-like conditions.[6] In addition, most flow-cell studies involve the use of monopolar ion exchange

P.-W. Huang, A. J. Medford
School of Chemical and Biomolecular Engineering
Georgia Institute of Technology
Atlanta, GA 30332, USA

H. Song
George W. Woodruff School of Mechanical Engineering
Georgia Institute of Technology
Atlanta, GA 30332, USA

J. Yoo, H. M. Lee
Department of Materials Science and Engineering
KAIST
291 Daehak-ro, Yuseong-gu, Daejeon 34141, Republic of Korea

D. A. Chipoco Haro
School of Materials Science and Engineering
Georgia Institute of Technology
Atlanta, GA 30332, USA

M. C. Hatzell
George W. Woodruff School of Mechanical Engineering and School of Chemical and Biomolecular Engineering
Georgia Institute of Technology
Atlanta, GA 30332, USA
E-mail: marta.hatzell@me.gatech.edu

The ORCID identification number(s) for the author(s) of this article can be found under https://doi.org/10.1002/aenm.202304202

DOI: 10.1002/aenm.202304202

membranes (Table S1, Supporting Information), namely anion exchange membranes (AEM) and cation exchange membranes (CEM). The use of AEM can result in the crossover of anions (e.g., nitrate and nitrite), while the use of CEM can result in crossover of cations (e.g., K^+, H^+, and NH_4^+). These unintended ionic crossovers can have detrimental impacts on the overall efficiency and economic viability of the electrochemical process.[6a,7] These challenges underscore a significant knowledge gap that must be addressed before NO_3RR can progress towards commercialization.

The conversion of NO_3^- to NH_3 involves a stepwise reduction process with multiple intermediates, resulting in the production of various reduced nitrogen compounds (e.g., NO_2^-, N_2, and NH_3).[3a] Thus it is challenging to achieve high selectivity towards NH_3. Most research attempts to address this via material design.[8] However, recent studies suggested that the concentration of protons is important for NO_3RR to be selective NH_3 production, especially in alkaline or neutral conditions.[9] Under these conditions, the direct reduction pathway (driven by H^+ from the electrolyte) is suppressed, which is detrimental to NH_3 formation. These findings indicate that maintaining a stable and well-regulated supply of protons is essential for achieving highly selective NH_3 production in wastewater conditions. Nevertheless, the impact of proton availability in NO_3RR has not yet been widely examined, even though wastewater typically has a pH between 7 and 12.[2]

The incorporation of bipolar membrane (BPM) with the membrane electrode assembly (MEA) system represents a potential strategy to overcome the obstacles associated with the current development of NO_3RR for NH_3 production. Compared to H-type cells, MEAs allow for higher current density studies and closely resemble commercial electrochemical cells, making MEA cell performance more representative of real-world applications.[6a,10] The BPM consists of a polymeric cation-exchange layer (CEL) and a polymeric anion-exchange layer (AEL), which has been proven to effectively prevent the crossover of ions and products during electrolysis.[6,11] By applying voltage, water dissociation occurs at the interface of the CEL and AEL, generating protons (H^+) and hydroxide ions (OH^-) simultaneously. Once generated, these ions undergo selective transport in the opposite direction, with H^+ passing through the CEL and OH^- passing through the AEL. Recently, the use of BPM has gained increasing attention in the field of (bi)carbonate electrolysis.[12] By operating the BPM-MEA system in a "reverse bias" fashion, with the CEL oriented towards the cathode, it enables the construction of stable proton flux from the BPM toward the cathode. This proton flux can be controlled by the introduction of gaps or additive layers between the BPM and electrode.[13] This adjustable proton flux could serve as a regulator to modify the product selectivity in NO_3RR. Nevertheless, research exploring the application of BPM-MEA systems for NO_3RR remains limited.[6b]

Here, we examined the NO_3RR within a BPM-MEA cell and specifically investigated how the proton availability can be tuned within the reactor to attain varied selectivity (NH_3 vs NO_2^- vs H_2). We investigate the impacts of an interposer layer (IPL) between the catalyst and membrane can have on the suppression of the hydrogen evolution reaction (HER).[13a] We also investigate the use of carbon capture-based solutions (0.5 M K_2CO_3), which function as a proton scavenger through the conversion of carbonate to CO_2 ($CO_3^{2-} + 2H^+ \rightarrow CO_2 + H_2O$). The integration of carbonate and IPL demonstrates synergistic effects in controlling proton flux, with the IPL creating a local pH gradient near the BPM that enhances both the conversion of carbonate to CO_2 and the consumption of protons. We also examine various reactor configurations to tune the mass transfer of reactants (e.g., NO_3^-, H^+, and CO_2). Finally, we carried out NO_3RR using an electrolyte that mimics wastewater conditions to assess the applicability of our BPM-MEA system in real-world scenarios. We demonstrate the feasibility of NO_3RR within a BPM-MEA system and propose a new MEA cell configuration that is favorable for NO_3RR under wastewater-like conditions. Through precise control of protons and the rational design of the cell configuration, high-selectivity NH_3 production can be achieved.

2. Results and Discussion

To date, there has been no systematic study of the NO_3RR within a BPM-MEA cell. We first evaluated the performance of the NO_3RR using a standard BPM-MEA reactor configuration (**Figure 1a**). In this cell, the BPM is flush with the anode and cathode. Commercial copper nanoparticles were chosen as the cathodic catalysts since copper is a widely discussed catalyst for NO_3RR,[8,14] which can ensure the reproducibility of our results. Scanning electron microscopy (SEM) and energy-dispersive X-ray spectroscopy (EDX) mapping revealed a uniform and well-distributed deposition of copper nanoparticles on carbon paper, as detailed in Figures S1 and S2, Supporting Information. A Ni foam serves as the anode (Figure 1a). Given that wastewater typically has a pH in the neutral to weak alkaline range (pH = 7-12) and contains 1000–9000 ppm of nitrate (NO_3-N),[2] 1 M KCl (pH = 7) was chosen as the catholyte, with the addition of approximately 1000 ppm NO_3-N (70×10^{-3} M KNO_3) to serve as the nitrogen source. Meanwhile, 1 M KOH was added to the counterpart as the anolyte. On the cathode side, the nitrate-containing electrolyte flows along the flow pattern, with nitrate permeating through the carbon paper to reach the copper catalyst where the NO_3RR occurs.

When conducting electrolysis in 1 M KCl, the HER dominates catalytic activity (FE_{HER} = 49.7% at 25 mA cm^{-2}). With an increase in current density, this selectivity toward hydrogen plateau around 80% in the range of 100 to 200 mA cm^{-2} (Figure 1b). The high HER competes with NO_3RR, leading to low NH_3 FE (Figure S3, Supporting Information) and indicating an excessive proton concentration in this condition. To identify the origin of HER, we conducted electrolysis in a higher pH environment (pH 12 and 14). The results show that, unless the bulk electrolyte is extremely alkaline (e.g., pH 14), the bulk pH does not strongly affect the HER in this BPM-MEA system, which suggests that the proton flux from BPM is the primary hydrogen source that leads to high HER (Figure S4, Supporting Information). To mitigate the excessive proton flux from BPM, we introduced a mixed cellulose ester (MCE) membrane filter between the BPM and Cu electrode as an IPL, a recognized approach in BPM-based CO_2 electrolysis for suppressing HER (Figure 1c).[13a] This additive layer functions by inhibiting proton transfer from the BPM to the Cu catalyst, resulting in varying levels of HER suppression at different current densities in 1 M KCl (Figure 1b). However, as the proton flux increases when applying higher current densities

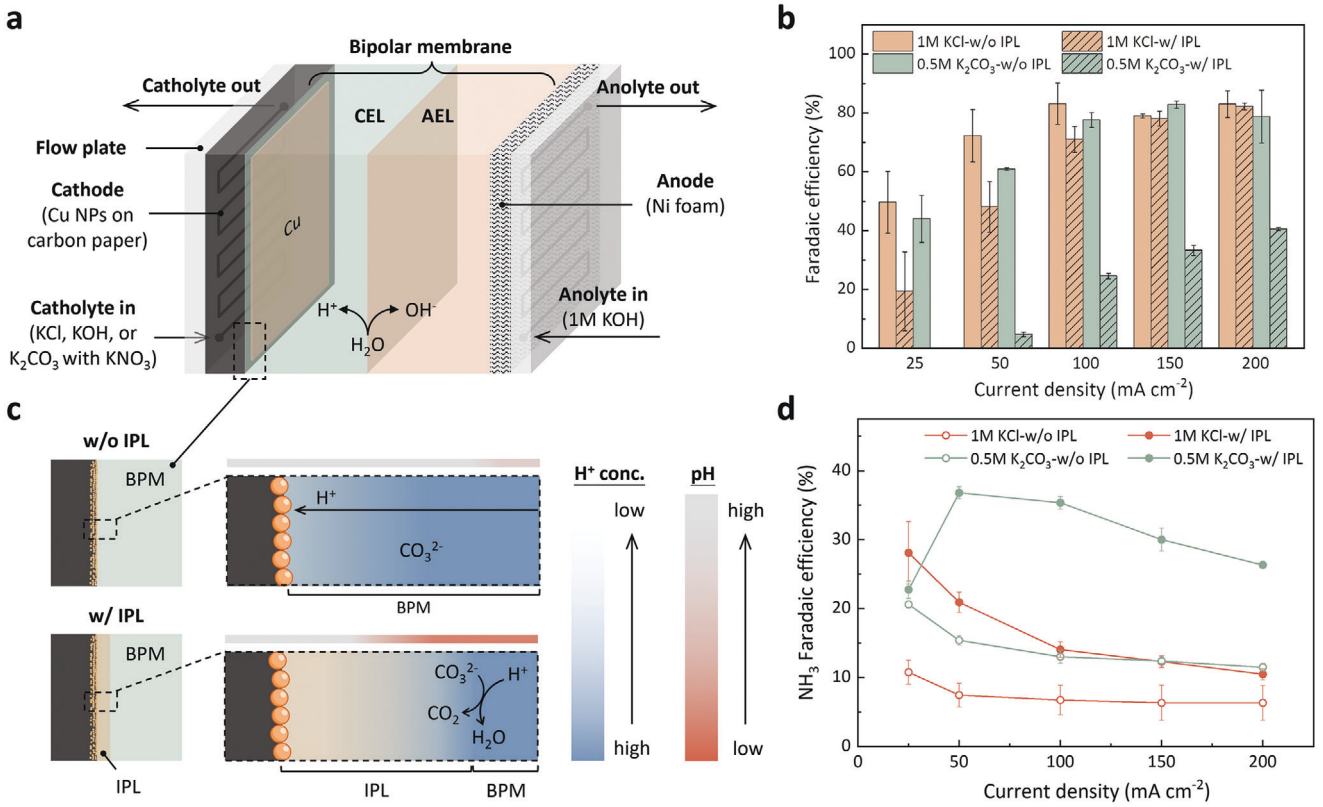

Figure 1. a) Schematic representation of a bipolar membrane (BPM) based membrane electrode assembly (MEA) electrolyzer. b) Hydrogen evolution reaction (HER) Faradaic efficiency (FE) in 1 M KCl and 0.5 M K_2CO_3 electrolytes containing 70×10^{-3} M KNO_3 across applied current densities ranging from 25 to 200 mA cm^{-2}. Bars with diagonal stripes indicate electrolysis with the presence of an interposer layer (IPL). c) Simplified illustration of the pH gradient within the IPL and its impact on proton inhibition in the BPM-MEA system. d) Ammonia FE in 1 M KCl and 0.5 M K_2CO_3 electrolytes containing 70×10^{-3} M KNO_3 with and without the presence of IPL across applied current densities ranging from 25 to 200 mA cm^{-2}. Error bars represent standard deviations from three repeated measurements.

(100–200 mA cm^{-2}), the inhibitory effect of the IPL on proton transfer becomes less pronounced. To tackle the issue of high HER at elevated currents, we introduced carbonate (in the form of K_2CO_3) into our system as a proton scavenger. In a proton-rich environment, carbonate undergoes conversion into CO_2 ($CO_3^{2-} + 2H^+ \rightarrow CO_2 + H_2O$), which consumes protons and potentially aids in the suppression of HER. The results indicate that the proton-blocking effects of both IPL (denoted as 1 M KCl-w/ IPL) and carbonate (denoted as 0.5 M K_2CO_3-w/o IPL) are limited at high current densities (Figure 1b). However, when combining IPL with carbonate (denoted as 0.5 M K_2CO_3-w/ IPL), the proton flux is notably suppressed. The HER is controlled at around 40% FE at 200 mA cm^{-2}, representing a 50% reduction in HER compared to 1 M KCl-w/o IPL. The pronounced strengthening of the proton-blocking effect can be ascribed to the synergistic effect arising from the incorporation of K_2CO_3 and an IPL. The implementation of the IPL not only hinders proton transfer but also introduces a local pH gradient near the BPM.[13a] This acidic microenvironment facilitates the proton scavenger effect by promoting the conversion of carbonate into CO_2, which aids in the consumption of protons. (Figure 1c). The result is consistent with findings in the field of CO_2 reduction reaction (CO_2RR), where a prior study reported that a significant pH shift occurs near the BPM when applying IPL to the BPM electrolysis system.[13a] This initiated a pH swing process that generated CO_2 from the carbonate solution (near the interface of IPL and BPM) while maintaining an alkaline environment at the catalyst side (i.e., the bulk pH).[13a] It is worth noting that the in situ generated CO_2 may also participate in the electrolysis (15.7% FE toward carbon products at 200 mA cm^{-2}) (Figure S5, Supporting Information). However, once generated CO_2 encounters the bulk electrolyte (alkaline solution), it converts back into carbonate, as supported by the detection of only trace levels of CO_2 during the experiment.

Due to the suppression of HER, the formation of NH_3 increased, with samples containing IPLs (1 M KCl-w/ IPL & 0.5 M K_2CO_3-w/ IPL) exhibiting higher NH_3 production than samples without the presence of IPLs (1 M KCl-w/o IPL & 0.5 M K_2CO_3-w/o IPL), and 0.5 M K_2CO_3-w/ IPL demonstrates the highest NH_3 FE (Figure 1d). The NH_3 FE decreases as the current density increases in all cases, except for 0.5 M K_2CO_3-w/ IPL. In 0.5 M K_2CO_3-w/ IPL, NH_3 production experiences a notable improvement from 25 to 50 mA cm^{-2}, reaches a plateau, and gradually decreases with higher current density. The low NH_3 production at low current density can be attributed to the limited availability of protons, aligned with the observation of no HER when applying 25 mA cm^{-2} (Figure 1b). The sharp increase in NH_3 production at 50 mA cm^{-2} supports the hypothesis that a moderate proton supply is essential for ammonia synthesis.

The results suggest that the product selectivity of NO_3RR in the BPM-MEA system is highly dependent on the local environment, and we have demonstrated that the reactants (i.e., proton flux and in situ generated CO_2) associate with undesired side reactions exhibit strong directionality (from BPM to flow plate) within the BPM-MEA system. Based on these findings, we reconfigured the MEA cell with the Cu electrodes facing away from the BPM (toward the flow plate), denoted as the reverse configuration (**Figure** 2a), and carried out electrolysis to investigate the influences of electrode orientation on NO_3RR performance (Figure 2b–d). The reverse configuration demonstrates a remarkable ability to suppress HER (Figure 2b). Without the presence of an IPL, the reverse configuration (reverse-w/o IPL) exhibits H_2 production similar to the forward configuration with the presence of IPL (forward-w/ IPL), while no H_2 formation can be observed from 25 to 150 mA cm^{-2}, and the HER FE is <9% at 200 mA cm^{-2} when applying IPL (reverse-w/ IPL). The Cu electrodes remain stable after electrolysis in both configurations, confirmed by SEM, EDX mapping, and X-ray photoelectron spectroscopy (XPS) (Figures S1, S2, and S6, Supporting Information).

Such a configuration and the associated performance changes may seem counterintuitive at first glance; however, this is related to the transfer of ions and/or reactants during electrochemical reactions (Figure 2a). In a standard electrochemical cell setup, the cathode and anode face each other (forward configuration), reducing the distance for ion transfer and thus lowering the ohmic resistance in the cell for electrochemical energy storage applications.[10c,15] In electrocatalysis research using an H-type cell, the diffusion of reactants is, in principle, non-directional, so the performance will not be markedly affected whether in a reverse or forward configuration. However, in the BPM-MEA system, the reactants (for example, nitrate in NO_3RR) are supplied from the flow plate, while protons are sourced from the BPM, creating a divergent transport path. In a standard setup (forward configuration), nitrate needs to diffuse through the substrate (in this case, carbon paper) to reach the Cu catalyst where the reduction reaction occurs, which, in turn, increases its diffusion resistance (Figure 2a). In the reverse setting, the resistance of nitrate diffusion decreases, while the diffusion length for protons and CO_2 increases, which is beneficial for NO_3RR. As a result, both HER and CO_2RR were highly inhibited (Figure 2c), with CO_2RR nearly vanishing. Furthermore, the cell voltage decreases when compared to the forward configuration, which serves as direct evidence that the resistance for NO_3RR is reduced in a reverse fashion (Figure S7, Supporting Information).

We have developed different methods (i.e., forward-w/ IPL, reverse-w/o IPL, and reverse-w/ IPL), which show varying degrees of HER suppression (Figure 2b). We then explore how the configurations alter NO_3RR selectivity for NH_3 over NO_2^- (Figure 2d). In all configurations, the selectivity increases with increasing current density. This can be attributed to the higher current density, where proton flux increases and creates proton-rich environments, promoting the formation of NH_3 over NO_2^- despite the elevated HER.[16] In the reverse-w/ IPL configuration, in the low current density region (<100 mA cm^{-2}), the selectivity is exceptionally low, primarily due to the excessive suppression of protons (Figure 2b), resulting in a more favorable formation of NO_2^-. Similar low selectivity performance can also be observed in other configurations when HER is low (both forward-w/ IPL and reverse-w/o IPL at 25 mA cm^{-2}). Subsequently, as the current density increases, the selectivity increases significantly in the reverse-w/ IPL configuration. This serves as strong evidence that moderate proton supply is crucial for NH_3 production. It is noteworthy that both the forward-w/ IPL and reverse-w/o IPL configurations exhibit comparable trends in selectivity (Figure 2d) as well as HER (Figure 2b), which further supports the notion that hydrogen plays an important role in selective NH_3 production.

To exclude the possibility of adventitious ammonia contamination that could lead to false positive results, the experiments were conducted rigorously, and all equipment (e.g., BPM, flow pattern, tubing, gasket, etc.) that might come into contact with the samples were rinsed with DI water before use.[17] Isotope labeling ^1H NMR spectroscopy was conducted (see Experimental Section). Due to its ability to distinguish between different isotopes (in this case, $^{14}NH_3$ and $^{15}NH_3$), isotope labeling NMR measurement is considered the most robust method to verify the nitrogen source for the measured NH_3.[18] The electrolytes for NMR measurement were collected after electrocatalytic reduction in the reverse-w/ IPL configuration. The NMR spectra show triplet peaks, which correspond to $^{14}NH_3$, when current is applied (200 mA cm^{-2}) and $^{14}NO_3^-$ was used as the nitrogen source (Figure 2e). When switching the nitrogen source to $^{15}NO_3^-$, the NMR spectra show clear doublet peaks, which correspond to the formation of $^{15}NH_3$, and no $^{14}NH_3$ peaks can be observed in this case. This indicates that the contamination level in our setup is low. To support this, control experiments without applying current were conducted (Figure 2e). The NMR spectra show that neither $^{14}NH_3$ nor $^{15}NH_3$ was detected, suggesting that contamination from nitrate and the system can be disregarded. Quantitative NMR measurements were performed using maleic acid as the internal reference. The NH_3 concentrations are very similar (<2% difference) when using either $^{15}NO_3^-$ or $^{14}NO_3^-$ as the nitrogen source and are consistent with the NH_3 measured by IC, further suggesting that the NH_3 measured in our experiments solely originates from NO_3RR.

We then investigated the NO_3RR performance of the reverse-w/ IPL configuration at elevated currents (**Figure** 3a). In line with the above discussion, as the current increases, the selectivity for NH_3 over NO_2^- continues to rise, as well as the production of H_2. As the competition between NO_3RR and HER intensified with the rising current, the performance reached its peak with an optimal NH_3 selectivity of 60.8% FE at an applied current density of 200 mA cm^{-2}, and the highest NH_3 partial current density achieved was 178.84 mA cm^{-2} at −7.89 V (Figure S8, Supporting Information).

The impact of carbonate concentration on NO_3RR was examined (Figures S9 and S10, Supporting Information), as carbonate solution plays an important role in our BPM-MEA system. As a proton scavenger, increasing the carbonate concentration leads to a decrease in H_2 formation (Figure 3b), which can be ascribed to the higher concentration of carbonate likely generating more CO_2, resulting in the consumption of more protons.[13a] Due to the superior proton regulation of 1 M K_2CO_3 compared to 0.5 M K_2CO_3, the peak of NH_3 FE shifts from 60.8% at 200 mA cm^{-2} to 61.0% at 250 mA cm^{-2} (Figure S10, Supporting Information). The claims that higher carbonate concentration generates more CO_2 can be supported by the observation of higher cell voltage in 1 M K_2CO_3 compared to 0.5 M K_2CO_3 (Figure 3b). The increased

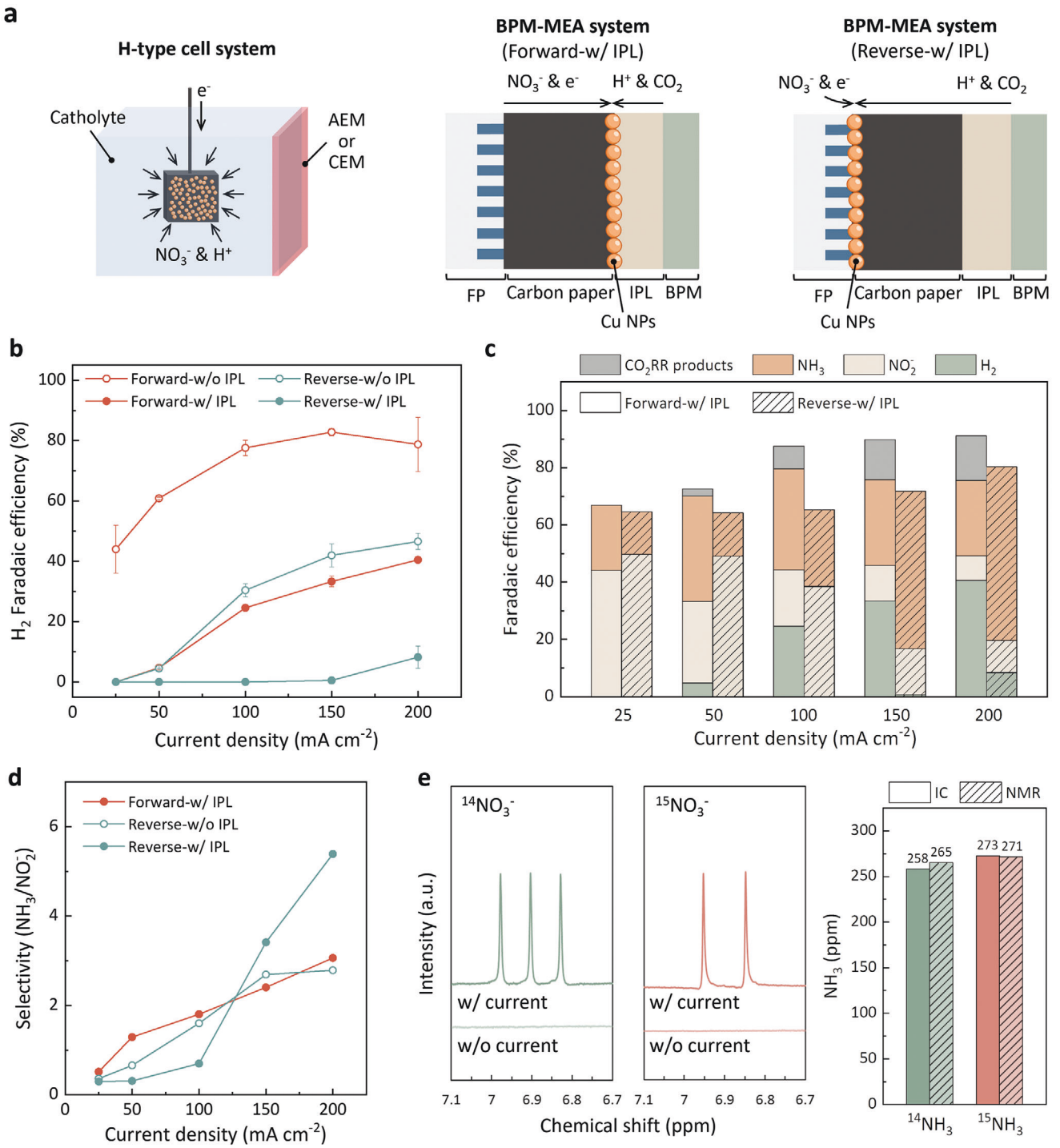

Figure 2. a) Simplified schematic of the mass transfer of reactants in different electrolyzer configurations. AEM: anion exchange membrane. CEM: cation exchange membrane. FP: flow plate. b) H_2 FE in 0.5 M K_2CO_3 electrolyte containing 70×10^{-3} M KNO_3 with electrode facing towards (forward-w/o IPL and forward-w/ IPL) and away (reverse-w/o IPL and reverse-w/ IPL) from the BPM. Error bars represent standard deviations from three repeated measurements. c) Product distribution of NO_3RR done with forward-w/ IPL and reverse-w/ IPL at varying applied current densities ranging from 25 to 200 mA cm^{-2}. The electrolysis was conducted in 0.5 M K_2CO_3 containing 70×10^{-3} M KNO_3. The CO_2RR products include C_2H_4, CH_4, $HCOO^-$, and CO. d) Ammonia-to-nitrite selectivity at forward and reverse configurations in 0.5 M K_2CO_3 containing 70×10^{-3} M KNO_3. e) Quantitative ammonia measurements using ionic chromatography (IC) and ^{1}H nuclear magnetic resonance (NMR) spectroscopy. The samples were collected after electrolysis with and without the applied of current (200 mA cm^{-2}) in electrolytes containing 70×10^{-3} M $K^{14}NO_3$ and $K^{15}NO_3$.

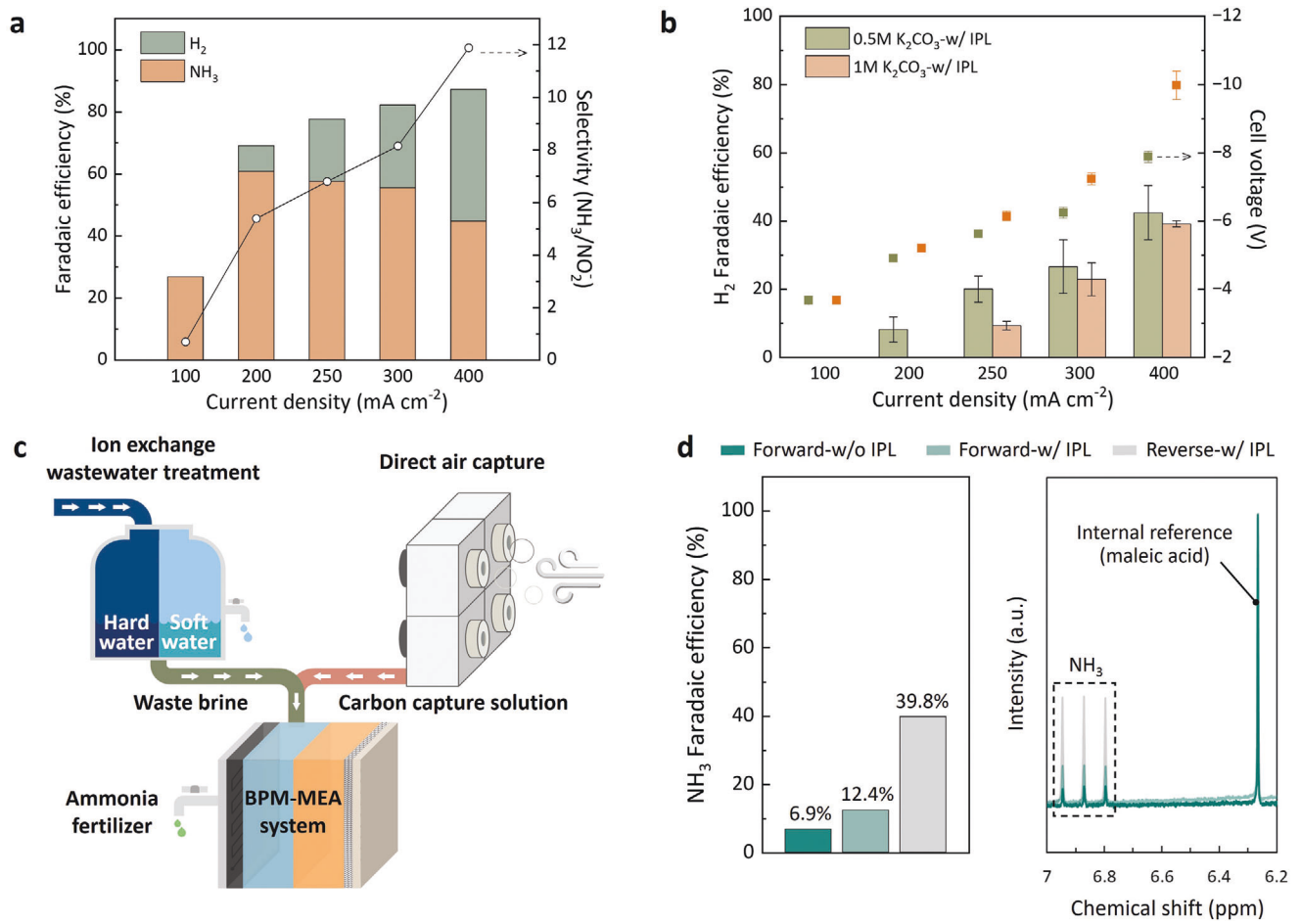

Figure 3. a) Performance metrics for ammonia and hydrogen production using the reverse-w/ IPL configuration at higher current densities ranging from 100 to 400 mA cm^{-2} in a 0.5 M K_2CO_3 solution containing 70×10^{-3} M KNO_3. The right-hand *y*-axis indicates the selectivity of ammonia to nitrite. b) H_2 FE and corresponding cell voltages measured in 0.5 and 1 M K_2CO_3 electrolytes with a nitrate concentration of 70×10^{-3} M using the reverse-w/ IPL system. Error bars represent standard deviations from three repeated measurements. c) Simplified diagram illustrating NO_3RR using the BPM-MEA system with nitrate-concentrated brine from ion exchange water treatment plants and carbon capture solution from the direct air capture facilities. d) Performance of ammonia production using synthetic wastewater as the catholyte in different electrolyzer configurations under applied current density at 200 mA cm^{-2}.

overpotential can be attributed to the in situ generation of CO_2, which forms tiny bubbles near the interface of IPL and BPM, leading to higher resistance.[13a] It is worth noting that even in the 1 M K_2CO_3 electrolyte, the electrolysis produces negligible carbon products (about 1% FE toward carbon products; Figure S11, Supporting Information). This finding suggests that CO_2 is well regulated in the reverse-w/ IPL configuration and reinforces the role of carbonate as a co-catalyst (proton scavenger) rather than a reactant, as it does not participate in the NO_3RR.

To gain a better understanding of the performance of the BPM-MEA cell in real-world conditions, we conducted electrolysis in a mimic wastewater solution. As a proof of concept, synthetic wastewater was prepared by mixing nitrate-concentrated brine from ion exchange water treatment plants (containing Na^+, K^+, Mg^{2+}, Cl^-, SO_4^{2-}, and NO_3^-) and carbon capture solution (1.5 M K_2CO_3) from direct air capture facilities in a volume ratio of 2:1 (Figure 3c; See Experimental Section).[2e,13a,19] Due to the presence of highly concentrated Na ions (1.4 M) in the mimic wastewater, quantitative ^1H NMR was used to measure NH_3, as the NH_3 peak overlaps with the Na^+ peak in IC under this specific condition. Compared to the standard MEA setup (forward-w/o IPL), the reverse-w/ IPL configuration exhibits stronger NH_3 characteristic peaks in the NMR spectra, corresponding to 167 ppm and 29 ppm of NH_3 after 30 min electrolysis in the reverse-w/ IPL and forward-w/o IPL configurations, respectively. At a current density of 200 mA cm^{-2}, the NH_3 FE, however, decreased to 39.8% compared to the 60.8% NH_3 FE achieved in pure 0.5 M K_2CO_3 electrolyte, despite the higher nitrate contents supplied in the mimic wastewater solution (100×10^{-3} M NO_3^- in the synthetic wastewater compared to 70×10^{-3} M NO_3^- in the 0.5 M K_2CO_3 electrolyte). The decrease in NH_3 FE may be associated with the detrimental effects of the complex interplay between the multi-ionic environment and active sites.[5b,20] Nevertheless, the results suggest that the reverse-w/ IPL configuration is more favorable for NH_3 production compared to the standard MEA setup (with an almost 6-fold increase in NH_3 yield) in wastewater-like conditions. This improvement can primarily be ascribed to the effective control of reactants transfer in the reverse-w/ IPL setup.

We expect that better performance can be achieved through optimization efforts, but the focal point of this work lies in emphasizing a fresh perspective: tackling the selective NH_3 production of NO_3RR from a cell design standpoint.

3. Conclusions

In conclusion, our research highlights the critical importance of moderate proton supply for achieving selective NH_3 production in NO_3RR. We employed various strategies (including IPL and proton scavenger) to modulate the proton flux and showcased their synergistic effect on proton regulation through integration. Furthermore, we proposed a new perspective on the configuration of BPM-based MEA cells for electrocatalytic studies, by evaluating the mass transfer limitations in current MEA setup. Quantitative isotope labeling NMR measurement was employed to ensure genuine ammonia production. By utilizing the new configuration, NH_3 yield has increased by 576% compared to the standard BPM-MEA setup in mimic wastewater solution, marking a significant advancement in NO_3RR. Future efforts can focus on optimizing performances, such as stability (Figure S12, Supporting Information) and energy efficiency (Figure S13, Supporting Information). These can be done by catalyst or membrane optimization. Furthermore, the potential applications of this system can be explored by adjusting the interlayers. For example, we observed variations in product distribution when introducing the Ag layer on the back side of the Cu electrode (Figure S14, Supporting Information). The strategies we developed here are universal (Figure S15, Supporting Information) and serve to regulate reactant transfer and local environments in BPM-based MEA cell electrolysis, which can be challenging to achieve in the setups of other electrochemical cells. We hypothesize that the BPM-MEA system we proposed can be utilized to investigate and optimize other electrochemical synthesis processes, such as the electrosynthesis of urea.[21]

Supporting Information

Supporting Information is available from the Wiley Online Library or from the author.

Acknowledgements

P.-W.H. and H.S. contributed equally to this work. This material is based upon work supported by the National Science Foundation under Grant No. 1846611 and 1933646. This work was supported by the Gordon and Betty Moore Foundation (Award 10615). This work was supported by the National Science Foundation through the Center for Advancing Sustainable and Distributed Fertilizer Production (CASFER) under Grant No. EEC-2133576.

Conflict of Interest

The authors declare no conflict of interest.

Data Availability Statement

The data that support the findings of this study are available in the supplementary material of this article.

Keywords

bipolar membrane, electrochemical nitrate reduction, hydrogen, membrane electrode assembly, product selectivity

Received: December 6, 2023
Revised: January 14, 2024
Published online:

[1] a) D. E. Canfield, A. N. Glazer, P. G. Falkowski, *Science* **2010**, *330*, 192; b) J. Lim, C. A. Fernández, S. W. Lee, M. C. Hatzell, *ACS Energy Lett.* **2021**, *6*, 3676; c) U. EPA, https://www.epa.gov/ground-water-and-drinking-water/national-primary-drinking-water-regulations (accessed: December 2024); d) P. H. van Langevelde, I. Katsounaros, M. T. M. Koper, *Joule* **2021**, *5*, 290; e) M. Duca, M. T. M. Koper, *Energy Environ. Sci.* **2012**, *5*, 9726.

[2] a) Á. Mayor, M. Reig, X. Vecino, J. L. Cortina, C. Valderrama, *Membranes* **2023**, *13*, 580; b) S. Guida, L. Van Peteghem, B. Luqmani, M. Sakarika, A. McLeod, E. J. McAdam, B. Jefferson, K. Rabaey, A. Soares, *Chem. Eng. J.* **2022**, *427*, 130896; c) J. Martínez, A. Ortiz, I. Ortiz, *Appl. Catal., B* **2017**, *207*, 42; d) X. Huo, J. Vanneste, T. Y. Cath, T. J. Strathmann, *Water Res.* **2020**, *175*, 115688; e) J. M. Hutchison, J. L. Zilles, *Environ. Sci.: -Water Res. Technol.* **2018**, *4*, 1181.

[3] a) J. Lim, C.-Y. Liu, J. Park, Y.-H. Liu, T. P. Senftle, S. W. Lee, M. C. Hatzell, *ACS Catal.* **2021**, *11*, 7568; b) R. Jia, Y. Wang, C. Wang, Y. Ling, Y. Yu, B. Zhang, *ACS Catal.* **2020**, *10*, 3533.

[4] a) X. Lu, J. Yu, J. Cai, Q. Zhang, S. Yang, L. Gu, G. I. N. Waterhouse, S.-Q. Zang, B. Yang, S. Lu, *Cell Rep. Phys. Sci.* **2022**, *3*, 100961; b) Q. Liu, Q. Liu, L. Xie, Y. Ji, T. Li, B. Zhang, N. Li, B. Tang, Y. Liu, S. Gao, Y. Luo, L. Yu, Q. Kong, X. Sun, *ACS Appl. Mater. Interfaces* **2022**, *14*, 17312; c) Y. Guo, R. Zhang, S. Zhang, Y. Zhao, Q. Yang, Z. Huang, B. Dong, C. Zhi, *Energy Environ. Sci.* **2021**, *14*, 3938; d) Z. Fang, Z. Jin, S. Tang, P. Li, P. Wu, G. Yu, *ACS Nano* **2022**, *16*, 1072; e) O. Peng, Q. Hu, X. Zhou, R. Zhang, Y. Du, M. Li, L. Ma, S. Xi, W. Fu, Z.-X. Xu, C. Cheng, Z. Chen, K. P. Loh, *ACS Catal.* **2022**, *12*, 15045; f) L. Mi, Q. Huo, J. Cao, X. Chen, H. Yang, Q. Hu, C. He, *Adv. Energy Mater.* **2022**, *12*, 2202247.

[5] a) J. Lim, Y. Chen, D. A. Cullen, S. W. Lee, T. P. Senftle, M. C. Hatzell, *ACS Catal.* **2023**, *13*, 87; b) I. Katsounaros, G. Kyriacou, *Electrochim. Acta* **2007**, *52*, 6412; c) F.-Y. Chen, Z.-Y. Wu, S. Gupta, D. J. Rivera, S. V. Lambeets, S. Pecaut, J. Y. T. Kim, P. Zhu, Y. Z. Finfrock, D. M. Meira, G. King, G. Gao, W. Xu, D. A. Cullen, H. Zhou, Y. Han, D. E. Perea, C. L. Muhich, H. Wang, *Nat. Nanotechnol.* **2022**, *17*, 759; d) Y. Wang, M. Sun, J. Zhou, Y. Xiong, Q. Zhang, C. Ye, X. Wang, P. Lu, T. Feng, F. Hao, F. Liu, J. Wang, Y. Ma, J. Yin, S. Chu, L. Gu, B. Huang, Z. Fan, *Proc. Natl. Acad. Sci. USA* **2023**, *120*, e2306461120.

[6] a) S. Li, D. Han, G. Jiang, Z. Han, H. Lu, J. Gao, X. Wang, Y. Wang, C. Geng, Z. Weng, Q.-H. Yang, *ACS Appl. Energy Mater.* **2023**, *6*, 5067; b) Z. Xu, L. Wan, Y. Liao, M. Pang, Q. Xu, P. Wang, B. Wang, *Nat. Commun.* **2023**, *14*, 1619.

[7] W. Bi, E. Gyenge, D. P. Wilkinson, *Chem. Eng. J.* **2023**, *478*, 147359.

[8] Y. Xiong, Y. Wang, J. Zhou, F. Liu, F. Hao, Z. Fan, *Adv. Mater.* **2023**, 2304021 https://onlinelibrary.wiley.com/doi/full/10.1002/adma.202304021.

[9] a) J. Gao, B. Jiang, C. Ni, Y. Qi, X. Bi, *Chem. Eng. J.* **2020**, *382*, 123034; b) X. Zou, J. Xie, C. Wang, G. Jiang, K. Tang, C. Chen, *Chin. Chem. Lett.* **2023**, *34*, 107908; c) R. Zhang, C. Li, H. Cui, Y. Wang, S. Zhang, P. Li, Y. Hou, Y. Guo, G. Liang, Z. Huang, C. Peng, C. Zhi, *Nat. Commun.* **2023**, *14*, 8036; d) J. M. McEnaney, S. J. Blair, A. C. Nielander, J. A. Schwalbe, D. M. Koshy, M. Cargnello, T. F. Jaramillo, *ACS Sustainable Chem. Eng.* **2020**, *8*, 2672.

[10] a) X. Fu, J. Zhang, Y. Kang, *Chem. Catal.* **2022**, *2*, 2590; b) S. C. Perry, P.-k. Leung, L. Wang, C. Ponce de León, *Curr. Opin. Electrochem.* **2020**, *20*, 88; c) S. Liang, N. Altaf, L. Huang, Y. Gao, Q. Wang, *J. CO2 Util.* **2020**, *35*, 90.

[11] a) M. A. Blommaert, J. A. H. Verdonk, H. C. B. Blommaert, W. A. Smith, D. A. Vermaas, *ACS Appl. Energy Mater.* **2020**, *3*, 5804; b) Y. C. Li, Z. Yan, J. Hitt, R. Wycisk, P. N. Pintauro, T. E. Mallouk, *Adv. Sustainable Syst.* **2018**, *2*, 1700187.

[12] a) A. J. Welch, E. Dunn, J. S. DuChene, H. A. Atwater, *ACS Energy Lett.* **2020**, *5*, 940; b) Y. C. Li, G. Lee, T. Yuan, Y. Wang, D.-H. Nam, Z. Wang, F. P. García de Arquer, Y. Lum, C.-T. Dinh, O. Voznyy, E. H. Sargent, *ACS Energy Lett.* **2019**, *4*, 1427; c) T. Li, E. W. Lees, M. Goldman, D. A. Salvatore, D. M. Weekes, C. P. Berlinguette, *Joule* **2019**, *3*, 1487.

[13] a) G. Lee, A. S. Rasouli, B.-H. Lee, J. Zhang, D. H. Won, Y. C. Xiao, J. P. Edwards, M. G. Lee, E. D. Jung, F. Arabyarmohammadi, H. Liu, I. Grigioni, J. Abed, T. Alkayyali, S. Liu, K. Xie, R. K. Miao, S. Park, R. Dorakhan, Y. Zhao, C. P. O'Brien, Z. Chen, D. Sinton, E. Sargent, *Joule* **2023**, *7*, 1277; b) Z. Yan, J. L. Hitt, Z. Zeng, M. A. Hickner, T. E. Mallouk, *Nat. Chem.* **2021**, *13*, 33; c) K. Xie, R. K. Miao, A. Ozden, S. Liu, Z. Chen, C.-T. Dinh, J. E. Huang, Q. Xu, C. M. Gabardo, G. Lee, J. P. Edwards, C. P. O'Brien, S. W. Boettcher, D. Sinton, E. H. Sargent, *Nat. Commun.* **2022**, *13*, 3609.

[14] a) M. Karamad, T. J. Goncalves, S. Jimenez-Villegas, I. D. Gates, S. Siahrostami, *Faraday Discuss.* **2023**, *243*, 502; b) W. Chen, X. Yang, Z. Chen, Z. Ou, J. Hu, Y. Xu, Y. Li, X. Ren, S. Ye, J. Qiu, J. Liu, Q. Zhang, *Adv. Funct. Mater.* **2023**, *33*, 2300512.

[15] J. Cabana, T. Alaan, G. W. Crabtree, P.-W. Huang, A. Jain, M. Murphy, J. N'Diaye, K. Ojha, G. Agbeworvi, H. Bergstrom, S. Gersib, H. Harb, A. Stejer, G. Quiles-Galarza, O. Rodriguez, I. Caruso, J. M. Gonçalves, G. Y. Chen, C. A. Fernández, H. Pan, K. Ritter, Y. Yang, H. Zhang, A. C. García-Álvarez, S. Ilic, K. Kumar, R. Silcox, Y. Yao, H. Song, S. Stoyanov, et al., *ACS Energy Lett.* **2023**, *8*, 740.

[16] R. Yang, H. Li, J. Long, H. Jing, X. Fu, J. Xiao, *ACS Sustainable Chem. Eng.* **2022**, *10*, 14343.

[17] a) P.-W. Huang, M. C. Hatzell, *Nat. Commun.* **2022**, *13*, 7908; b) H. Iriawan, S. Z. Andersen, X. Zhang, B. M. Comer, J. Barrio, P. Chen, A. J. Medford, I. E. L. Stephens, I. Chorkendorff, Y. Shao-Horn, *Nat. Rev. Methods Primers* **2021**, *1*, 56; c) J. Choi, B. H. R. Suryanto, D. Wang, H.-L. Du, R. Y. Hodgetts, F. M. Ferrero Vallana, D. R. MacFarlane, A. N. Simonov, *Nat. Commun.* **2020**, *11*, 5546.

[18] S. Z. Andersen, V. Čolić, S. Yang, J. A. Schwalbe, A. C. Nielander, J. M. McEnaney, K. Enemark-Rasmussen, J. G. Baker, A. R. Singh, B. A. Rohr, M. J. Statt, S. J. Blair, S. Mezzavilla, J. Kibsgaard, P. C. K. Vesborg, M. Cargnello, S. F. Bent, T. F. Jaramillo, I. E. L. Stephens, J. K. Nørskov, I. Chorkendorff, *Nature* **2019**, *570*, 504.

[19] A. Rinberg, A. M. Bergman, D. P. Schrag, M. J. Aziz, *ChemSusChem* **2021**, *14*, 4439.

[20] a) G. Horányi, E. M. Rizmayer, *J. Electroanal. Chem. Interfacial Electrochem.* **1982**, *140*, 347; b) D. Pletcher, Z. Poorabedi, *Electrochim. Acta* **1979**, *24*, 1253.

[21] H. Song, D. A. Chipoco Haro, P.-W. Huang, L. Barrera, M. C. Hatzell, *Acc. Chem. Res.* **2023**, *56*, 2944.